

This is a self-archived version of an original article. This version may differ from the original in pagination and typographic details.

Author(s): Altowyan, Mezna Saleh; Soliman, Saied M.; Haukka, Matti; Al-Shaalan, Nora Hamad; Alkharboush, Aminah A.; Barakat, Assem

Title: [3+2] Cycloaddition Reaction for the Stereoselective Synthesis of a New Spirooxindole Compound Grafted Imidazo[2,1-b]thiazole Scaffold : Crystal Structure and Computational Study

Year: 2022

Version: Published version

Copyright: © 2021 by the authors. Licensee MDPI, Basel, Switzerland

Rights: CC BY 4.0




Rights url: <https://creativecommons.org/licenses/by/4.0/>

Please cite the original version:

Altowyan, M. S., Soliman, S. M., Haukka, M., Al-Shaalan, N. H., Alkharboush, A. A., & Barakat, A. (2022). [3+2] Cycloaddition Reaction for the Stereoselective Synthesis of a New Spirooxindole Compound Grafted Imidazo[2,1-b]thiazole Scaffold : Crystal Structure and Computational Study. *Crystals*, 12(1), Article 5. <https://doi.org/10.3390/cryst12010005>

Article

[3+2] Cycloaddition Reaction for the Stereoselective Synthesis of a New Spirooxindole Compound Grafted Imidazo[2,1-*b*]thiazole Scaffold: Crystal Structure and Computational Study

Mezna Saleh Altowyan ¹, Saied M. Soliman ², Matti Haukka ³, Nora Hamad Al-Shaalan ¹, Aminah A. Alkharboush ¹ and Assem Barakat ^{4,*}

¹ Department of Chemistry, College of Science, Princess Nourah Bint Abdulrahman University, P.O. Box 84428, Riyadh 11671, Saudi Arabia; msaltowyan@pnu.edu.sa (M.S.A.); nhalshaal@pnu.edu.sa (N.H.A.-S.); Amina84w@gmail.com (A.A.A.)

² Department of Chemistry, Faculty of Science, Alexandria University, P.O. Box 426, Alexandria 21321, Egypt; saied1soliman@yahoo.com

³ Department of Chemistry, University of Jyväskylä, P.O. Box 35, FI-40014 Jyväskylä, Finland; matti.o.haukka@jyu.fi

⁴ Department of Chemistry, College of Science, King Saud University, P.O. Box 2455, Riyadh 11451, Saudi Arabia

* Correspondence: ambarakat@ksu.edu.sa; Tel.: +966-11467-5901; Fax: +966-11467-5992



Citation: Altowyan, M.S.; Soliman, S.M.; Haukka, M.; Al-Shaalan, N.H.; Alkharboush, A.A.; Barakat, A. [3+2] Cycloaddition Reaction for the Stereoselective Synthesis of a New Spirooxindole Compound Grafted Imidazo[2,1-*b*]thiazole Scaffold: Crystal Structure and Computational Study. *Crystals* **2022**, *12*, 5. <https://doi.org/10.3390/cryst12010005>

Academic Editor: Scott J. Dalgarno

Received: 1 December 2021

Accepted: 17 December 2021

Published: 21 December 2021

Publisher's Note: MDPI stays neutral with regard to jurisdictional claims in published maps and institutional affiliations.



Copyright: © 2021 by the authors. Licensee MDPI, Basel, Switzerland. This article is an open access article distributed under the terms and conditions of the Creative Commons Attribution (CC BY) license (<https://creativecommons.org/licenses/by/4.0/>).

Abstract: A new spirooxindole hybrid engrafted imidazo[2,1-*b*]thiazole core structure was designed and achieved via [3+2] cycloaddition reaction approach. One multi-component reaction between the ethylene derivative based imidazo[2,1-*b*]thiazole scaffold with 6-Cl-isatin and the secondary amine under heat conditions afforded the desired compound in a stereoselective manner. The relative absolute configuration was assigned based on single-crystal X-ray diffraction analysis. Hirshfeld calculations for **4** revealed the importance of the H...H (36.8%), H...C (22.9%), Cl...H (10.4%) and S...H (6.6%), as well as the O...H (4.7%), N...H (5.3%), Cl...C (1.6%), Cl...O (1.0%) and N...O (0.5%) contacts in the crystal stability. DFT calculations showed excellent straight-line correlations ($R^2 = 0.9776\text{--}0.9962$) between the calculated and experimental geometric parameters. The compound has polar nature (3.1664 Debye). TD-DFT and GIAO calculations were used to assign and correlate the experimental UV-Vis and NMR spectra, respectively.

Keywords: spirooxindole; imidazo[2,1-*b*]thiazole; azomethine ylide; [3+2] cycloaddition (32CA) reaction

1. Introduction

Imidazo [2,1-*b*]thiazole is an important bicyclic nitrogen and sulfur containing compound in some natural as well as synthetic pharmacologically active compounds and agrochemicals [1,2]. Many compounds reported in the literature incorporating imidazothiazole exhibited pharmaceutical targets such as antihelminthic [3], antifungal [4] and antibacterial [5], and also in cancer research development as anti-tumor agents [6–8]. Levamisolum is one of the representative pharmaceutically relevant molecules for immunomodulatory and antihelminthic agents which have partially hydrogenated imidazo[2,1-*b*]thiazole as a core constituent (Figure 1). Due to a drug-resistant bacterial infection and in the effort to develop a novel antimicrobial agent, Li et al. reported a new series of bicyclic incorporating dihydroimidazothiazole scaffold and exhibited high potency against methicillin-resistant *S. aureus* (MERSA) [9].

Indeed, Miyazaki et al. reported a lead compound comprising imidazo[2,1-*b*]thiazole scaffold for cancer treatment, targeting p53–MDM2 protein–protein interaction inhibitors [10].

The Éric Marsault and Emanuel Escher research group designed, synthesized and studied the biological evaluation of the imidazo[2,1-*b*]thiazole system against CXCR4 antagonists [11]. The chemical and biological studies of this privileged structure have gained a lot of attention from the researchers.

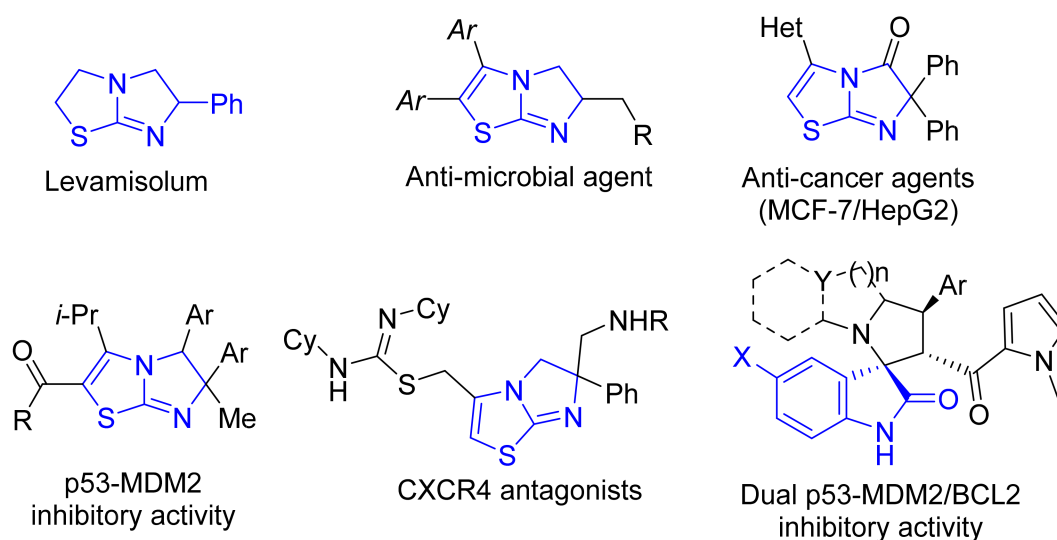


Figure 1. Representative examples of biologically active compounds having imidazothiazole and spirooxindole derivatives.

Spirooxindole is an important pharmacophore exhibiting a lot of pharmaceutical targets including anti-tumor [12], and anti-inflammatory targets [13], but also for treating Alzheimer's disease [14,15], and other pharmacological activity [16]. Recently, Barakat et al. reported a spirooxindole lead compound for cancer treatment targeting p53–MDM2 protein–protein interaction inhibitors [17,18]. The combination of these two spirooxindole and imidazo [2,1-*b*]thiazole pharmacophores may integrate the biological properties of both.

In the area of synthetic and medicinal chemistry research, multi-component reactions (MCRs) became important methodological arsenal as they were eco-friendly, had less reaction time, had a step-/atom economy and provided high-chemical yields. Additionally, for drug discovery and development, MCRs acted as an amenable tool for the generation of a library of new chemical entities. The [3+2] Cycloaddition (32CA) reaction [19–22] is a class of the multi-component reactions which afford a diversity of highly complex molecules efficiently and with a straightforward transformation.

In this text, we have reported the straightforward synthesis of a new compound having two pharmacophores based on the spirooxindole and imidazothiazole scaffolds *via* [3+2] cycloaddition (32CA) reaction. The crystal structure and the physical properties of the synthesized molecule were studied.

2. Materials and Methods

All technical instruments and chemicals used in this study are provided in the Supplementary Materials. The synthesis of imidazo[2,1-*b*]thiazole derivative 1 followed by the reported procedure [23].

*(2S,7a'S)-6''-Chloro-7'-(4-chlorophenyl)-5,6-diphenyl-7',7a'-dihydro-1'H,3H,3'H-dispiro [imidazo[2,1-*b*]thiazole-2,6'-pyrrolo[1,2-*c*]thiazole-5',3''-indoline]-2'',3-dione 4*

A mixture of imidazo[2,1-*b*]thiazole derivative 1 (207 mg, 0.5 mmol), 6-Cl-isatin (90.5 mg, 0.5 mmol) and (*R*)-thiazolidine-4-carboxylic acid (66.5 mg, 0.5 mmol) in methanol (10 mL)/dichloromethane (DCM) (10 mL) was refluxed on an oil bath for the appropriate time of 5 h. After the completion of the reaction as evident from TLC, the reaction was kept at room temperature overnight and the solid precipitate was filtered off without any

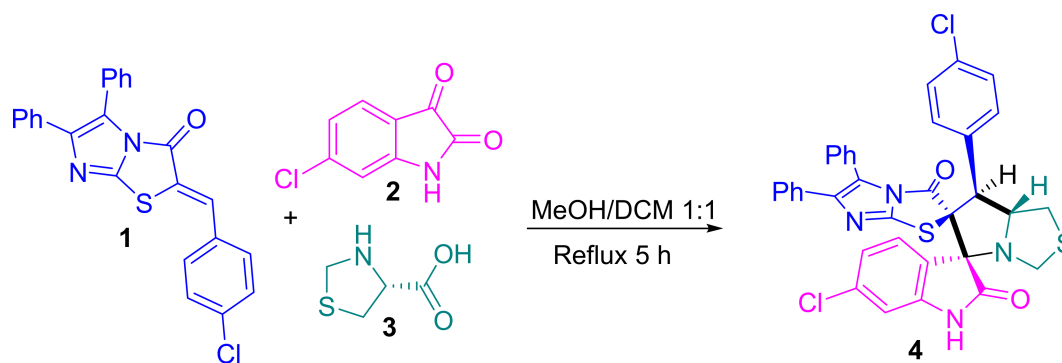
further purification in 92% chemical yield. Crystalline compound was obtained by slow evaporation in methanol.

^1H NMR (400 MHz, CDCl_3) δ 8.74 (s, 1H), 7.55–7.16 (m, 14H), 7.14 (d, J = 5.0 Hz, 1H), 6.98 (d, J = 8.0 Hz, 1H), 6.76 (s, 1H), 4.88 (q, J = 7.6 Hz, 1H), 4.15 (d, J = 9.0 Hz, 1H), 3.76 (d, J = 5.9 Hz, 1H), 3.58 (d, J = 5.9 Hz, 1H), 2.96 (dd, J = 9.8, 5.5 Hz, 1H), 2.84–2.73 (m, 1H); ^{13}C NMR (101 MHz, CDCl_3) δ 176.3, 168.7, 149.9, 146.1, 143.5, 137.3, 134.7, 134.6, 132.0, 131.5, 130.7, 129.5, 129.3, 128.7, 128.4, 128.4, 127.4, 127.3, 124.9, 123.1, 120.8, 111.7, 82.4, 75.7, 71.0, 56.2, 46.8, 32.9, 14.2; IR (KBr, cm^{-1}): 3419, 3318, 2921, 2855, 1730, 1620, 1511, 1210; Chemical Formula: $\text{C}_{35}\text{H}_{24}\text{Cl}_2\text{N}_4\text{O}_2\text{S}_2$.

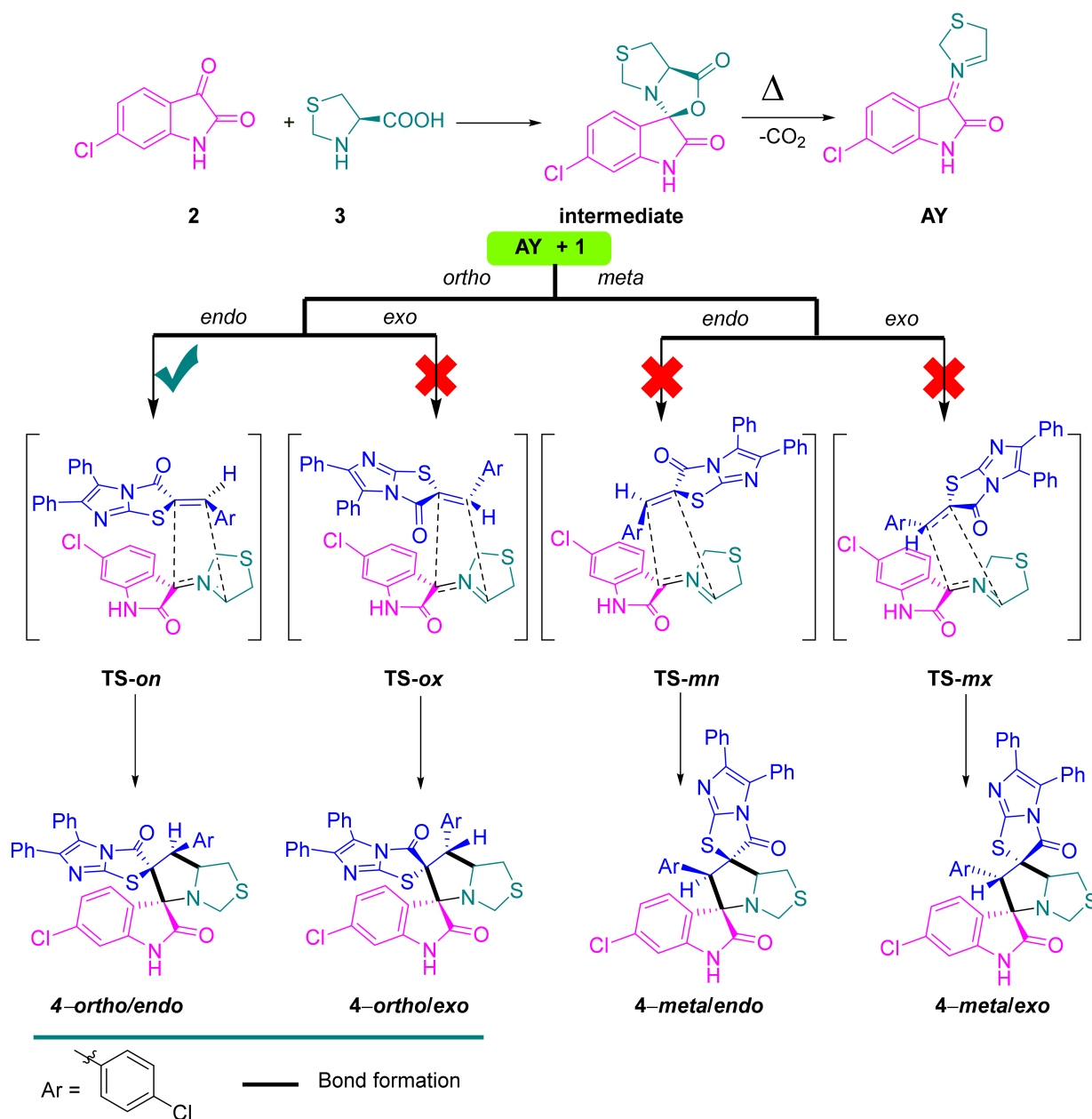
3. Results and Discussion

3.1. Chemistry

The target spirooxindole compound based imidazo[2,1-*b*]thiazole scaffold was designed and synthesized from the starting material named (*Z*)-2-(4-chlorobenzylidene)-5,6-diphenylimidazo[2,1-*b*]thiazol-3(2*H*)-one **1** with the 6-chloroisatin **2** and (*R*)-thiazolidine-4-carboxylic acid in MeOH/DCM (1:1) under reflux for 5 h (Scheme 1). The generated azomethine ylide was involved in the reaction as the intermediate which further moved to the [3+2] cycloaddition (32CA) reaction with the ethylene derivative based imidazo thiazole to afford the new *bis*-spiro compound **4** (Scheme 2). The transition states were proposed to afford the only regioisomer and diastereoisomer based on the recent literature [19–22,24] (Scheme 2). The chemical feature of the *bis*-spiro compound **4** was assigned based on ^1H -NMR, ^{13}C -NMR, IR and single-crystal X-ray diffraction analysis. The data analysis revealed that the chemical structure fully agreed with the designed structure. The ^1H -NMR spectrum showed the characteristic protons in the proposed structure as follows: NH proton assigned at δ 8.74 ppm as a singlet signal; in the aromatic region δ 7.55–7.16 ppm appeared for the overlapped 14 protons of the aromatic rings (two phenyl rings plus *p*-Cl-Ph); the three protons of the oxindole ring shown as two protons doublet and one proton singlet in the chemical shift at δ 7.14, 6.98 and 6.76 ppm, respectively. The protons of the fused cyclic ring appeared in the region between δ 4.88 until 2.73 ppm. ^{13}C -NMR spectrum exhibited the assigned carbons of the synthesized compound in very good manner. IR spectrum showed most functional groups existing in the proposed structure, such as NH, C-H, C=O, C=C, C=N, C-S, C-N, stretching as well as the pending vibrational assignment.



Scheme 1. Synthesis of spirooxindole based imidazo[2,1-*b*]thiazole scaffold **4**.



Scheme 2. Proposed approach of AY to ethylene derivative **1**, explaining the regio- and stereoselective synthesis of **4**.

3.2. Crystal Structure Description of **4**

The X-ray single-crystal structure analysis of **4** revealed the expected structure based on the spectral characterizations very well (Figure 2). The compound crystallized in a monoclinic crystal system and centrosymmetric $P2_1/c$ space group with lattice parameters: $a = 6.57040(10)$ Å, $b = 29.6357(5)$ Å, $c = 15.5008(4)$, $\beta = 96.898(2)^\circ$ (Table 1). The molecule comprised many ring systems, for more clarity these rings were designated as A to H as shown in Figure 2. The two fused rings A and B are nearly coplanar where both rings deviated from one another by 3.27° . Similarly, the two rings C and D deviated from one another by only 1.78° , indicating a coplanar fused-ring system. In contrast, the two fused five membered rings H and I are not perfectly coplanar where the perfectly planar parts of these rings are C8C7C19C11 and C8C9S1C10, respectively. It is clear that both rings have envelope conformation where the N atom is located out of the plane of each ring by distances of 0.700 and 0.644 Å, respectively. As expected, the three phenyl moieties are

perfectly planar where the two rings E and F make angles of 22.78 and 64.07° with the mean plane of C8C7C19C11 atoms. The molecular structure of this compound is stabilized by the three intramolecular C8-H8...O1, C1-H1...O1 and C17-H17...O2 with donor–acceptor distances of 2.953(2), 3.423(3) and 3.129(2) Å (Table 2). For better clarity, this hydrogen bonding interaction is presented as the turquoise-dotted line in the left part of Figure 3.

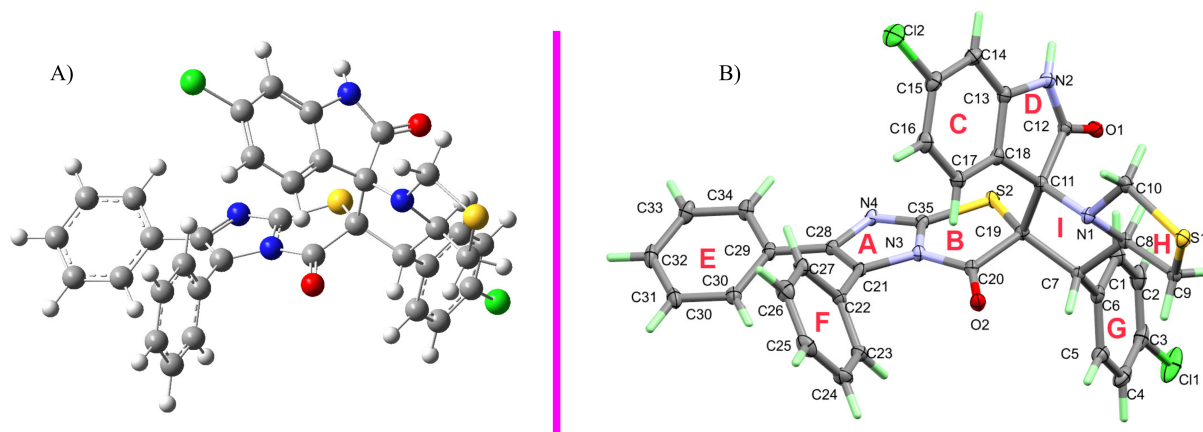


Figure 2. (A) AM1 semiempirical optimization (4-*ortho-endo*); (B) X-ray structure of 4.

Table 1. Crystal Data of compound 4.

Contact	4
CCDC	2075,962
empirical formula	C ₃₅ H ₂₄ Cl ₂ N ₄ O ₂ S ₂
fw	667.60
temp (K)	120(2)
λ (Å)	1.54184
cryst syst	Monoclinic
space group	<i>P</i> ₂ ₁ / <i>c</i>
<i>a</i> (Å)	6.57040(10)
<i>b</i> (Å)	29.6357(5)
<i>c</i> (Å)	15.5008(4)
α (deg)	90
β (deg)	96.898(2)
γ (deg)	90
<i>V</i> (Å ³)	2996.44(10)
<i>Z</i>	4
ρ _{calc} (Mg/m ³)	1.480
μ(Mo Kα) (mm ⁻¹)	3.589
No. reflns.	25,495
Unique reflns.	6231
GOOF (<i>F</i> ²)	1.025
<i>R</i> _{int}	0.0466
<i>R</i> ₁ ^a (<i>I</i> ≥ 2σ)	0.0400
<i>wR</i> ₂ ^b (<i>I</i> ≥ 2σ)	0.0975

^a $R_1 = \sum ||F_o| - |F_c|| / \sum |F_o|$. ^b $wR_2 = [\sum [w(F_o^2 - F_c^2)^2] / \sum [w(F_o^2)^2]]^{1/2}$.

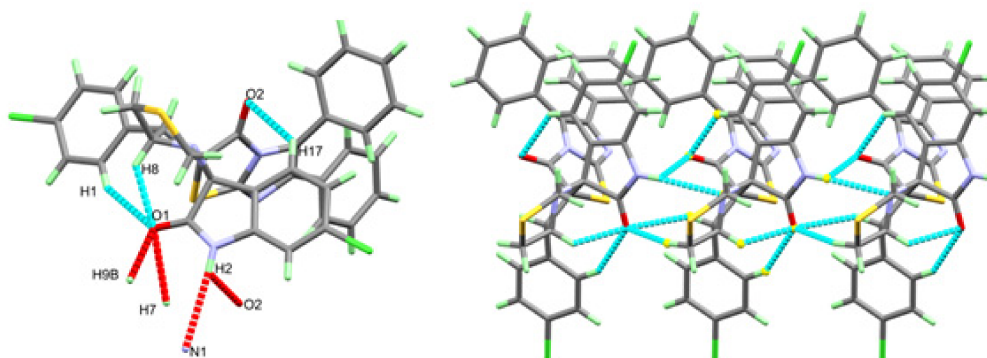


Figure 3. Hydrogen bond contacts in **4**.

The molecules of **4** are packed by three hydrogen bonds presented as red-dotted lines in Figure 3. The molecules are packed *via* strong N2-H2...O2 with donor–acceptor distances of 2.826(2) Å (Table 3). Additionally, the N2-H2...N1, C7-H7...O1 and C9-H9B...O1 have longer interactions distances of 3.470(3), 3.419(2) and 3.207(2) Å, respectively (Figure 3, right part).

Table 2. Hydrogen bond parameters (Å and °) for **4**.

D-H ... A	D-H	H ... A	D ... A	D-H ... A
N2-H2...O2 ¹	0.87(3)	2.50(3)	2.826(2)	103(2)
N2-H2...N1 ¹	0.87(3)	2.60(3)	3.470(3)	176(2)
C1-H1...O1	0.95	2.58	3.423(3)	147
C7-H7...O1 ²	1.00	2.55	3.419(2)	145
C8-H8...O1	1.00	2.23	2.953(2)	128
C9-H9B...O1 ²	0.99	2.25	3.207(2)	162
C17-H17...O2	0.95	2.40	3.129(2)	133

Symm. Code. ¹-1 + x,y,z; ²1 + x,y,z.

Table 3. Bond lengths (Å) and angles (°) for **4**.

Bond	Length/Å	Bond	Length/Å
C11-C3	1.744(2)	C8-C9	1.527(3)
C12-C15	1.738(2)	C11-C18	1.515(3)
S1-C10	1.828(2)	C11-C12	1.563(3)
S1-C9	1.846(2)	C11-C19	1.579(3)
S2-C35	1.741(2)	C13-C14	1.385(3)
S2-C19	1.8403(19)	C13-C18	1.394(3)
O1-C12	1.222(3)	C14-C15	1.387(3)
O2-C20	1.197(2)	C15-C16	1.386(4)
N1-C10	1.449(3)	C16-C17	1.396(3)
N1-C11	1.467(2)	C17-C18	1.389(3)
N1-C8	1.473(2)	C19-C20	1.541(3)
N2-C12	1.352(3)	C21-C28	1.368(3)
N2-C13	1.404(3)	C21-C22	1.478(3)
Bonds	Angle/°	Bonds	Angle/°
C10-S1-C9	93.42(9)	C16-C15-C12	119.00(18)
C35-S2-C19	91.24(9)	C14-C15-C12	118.04(19)
C10-N1-C11	119.55(16)	C15-C16-C17	119.4(2)
C10-N1-C8	108.89(16)	C18-C17-C16	119.3(2)
C11-N1-C8	105.30(15)	C17-C18-C13	119.11(19)
C12-N2-C13	110.93(17)	C17-C18-C11	132.67(19)
C35-N3-C20	116.22(16)	C13-C18-C11	108.03(17)
C35-N3-C21	106.91(16)	C20-C19-C11	107.31(15)
C20-N3-C21	135.89(17)	C20-C19-C7	108.93(15)
C35-N4-C28	104.18(16)	C11-C19-C7	104.53(15)

3.3. Analysis of Molecular Packing

The Hirshfeld surfaces of **4** are shown in Figure 4 while the intermolecular contacts are presented in Figure 5. The molecular packing is dominated by H...H (36.8%), H...C (22.9%), Cl...H (10.4%) and S...H (6.6%) contacts where the majority of these interactions have longer interaction distances than the vdWs radii sum of the interacting atoms except for the H...C contacts. In addition to the short H...C contacts, the packing is controlled by many other short contacts such as O...H (4.7%), N...H (5.3%), Cl...C (1.6%), Cl...O (1.0%) and N...O (0.5%) contacts. The shortest interactions along with the corresponding distances are listed in Table 4. Most of these interactions are short with characteristic sharp peaks in the fingerprint plot (Figure 6) and red regions in d_{norm} map indicating significant interactions (Figure 7).

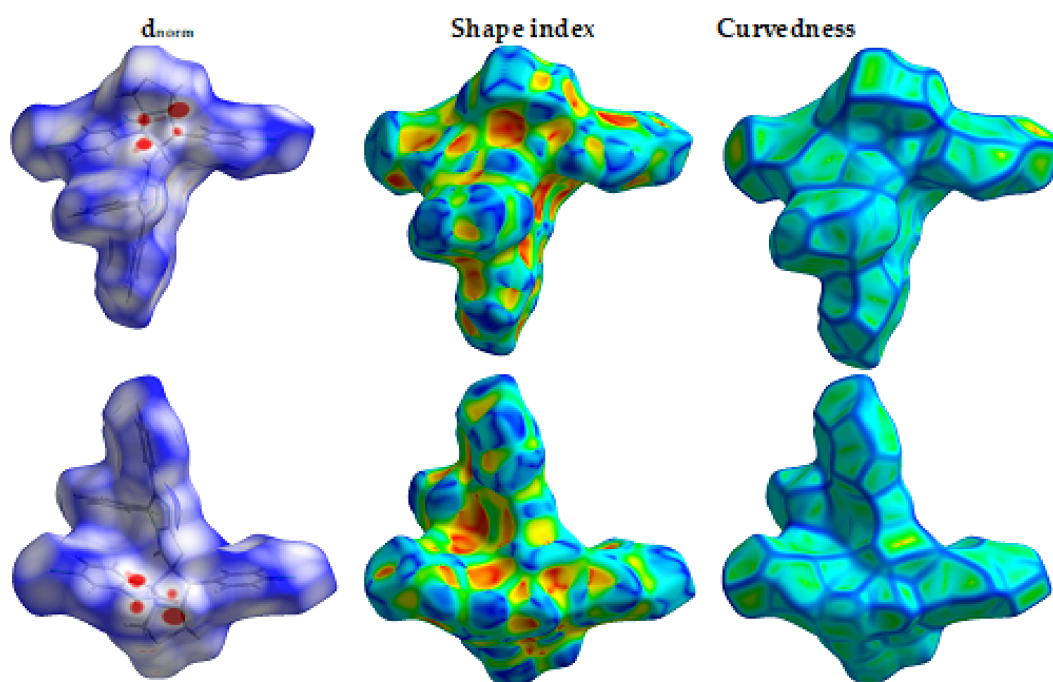


Figure 4. Hirshfeld surfaces of **4**.

Table 4. Intermolecular interactions and their distances in **4**^a.

Contact	Distance	Contact	Distance
N2...O2	2.826	N4...H23	2.631
C13...O2	3.16	N1...H2	2.463
O2...H2	2.476	H10B...C35	2.73
O1...H5	2.572	Cl1...C16	3.432
O1...H7	2.487	Cl1...Cl2 ^a	3.586
O1...H9B	2.162		

^a longer distances than the vdWs radii sum.

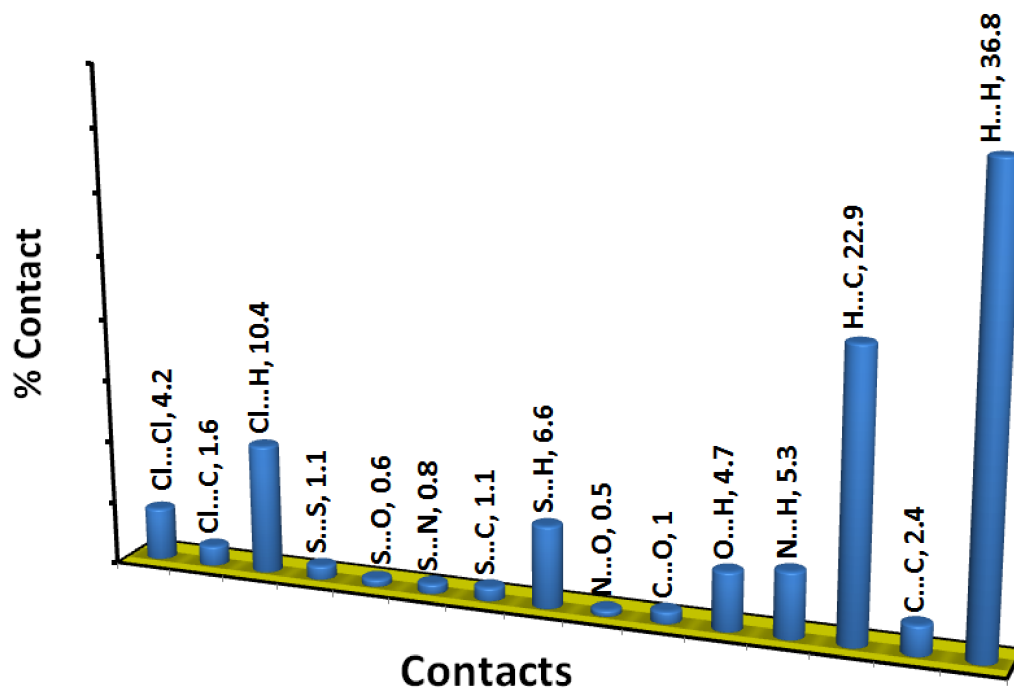


Figure 5. Intermolecular interactions in 4.

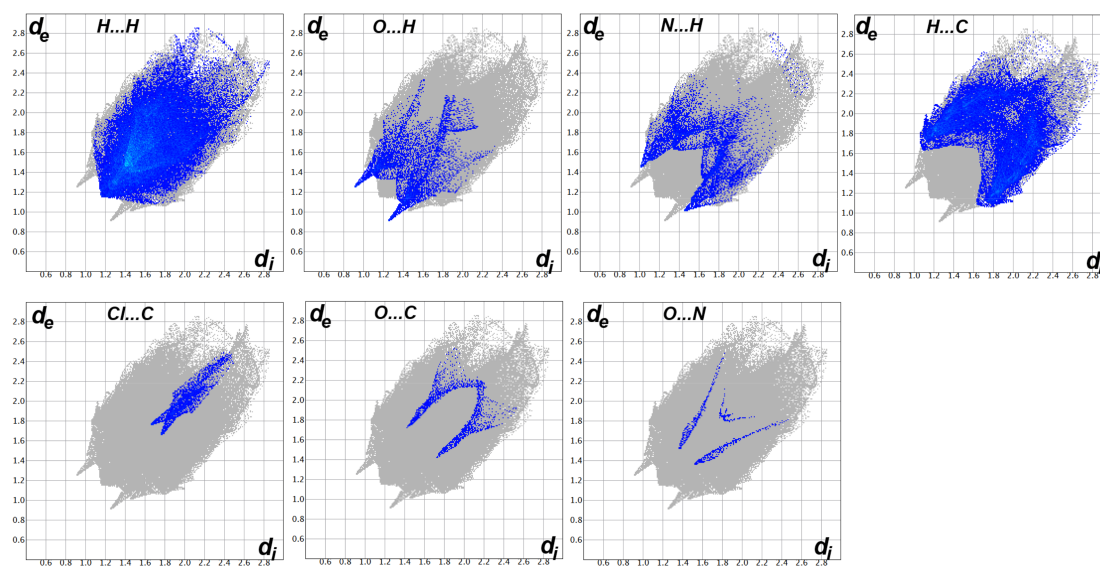


Figure 6. Decomposed fingerprint plots for the important interactions in 4.

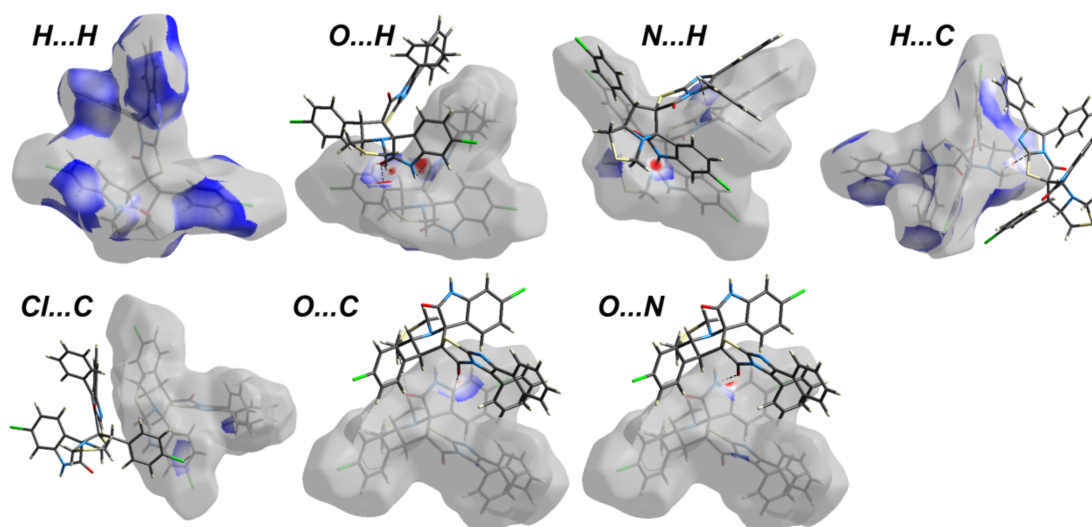


Figure 7. Decomposed d_{norm} surfaces for the important interactions in **4**.

3.4. DFT Studies

Using a B3LYP method, the structure of **4** was optimized (Figure 8). The computed structure of **4** showed good matching with the experimental geometry. The list of bond distances and angles depicted in Table S1 (Supplementary Data) reveal the good agreement between the calculations and the experiment. In this regard, the correlation graphs shown in Figure 9 indicated an excellent straight-line relation ($R^2 = 0.9776\text{--}0.9962$) between the calculated and experimental values. The presence of intermolecular interactions in the solid state could be the main reason for such deviations.

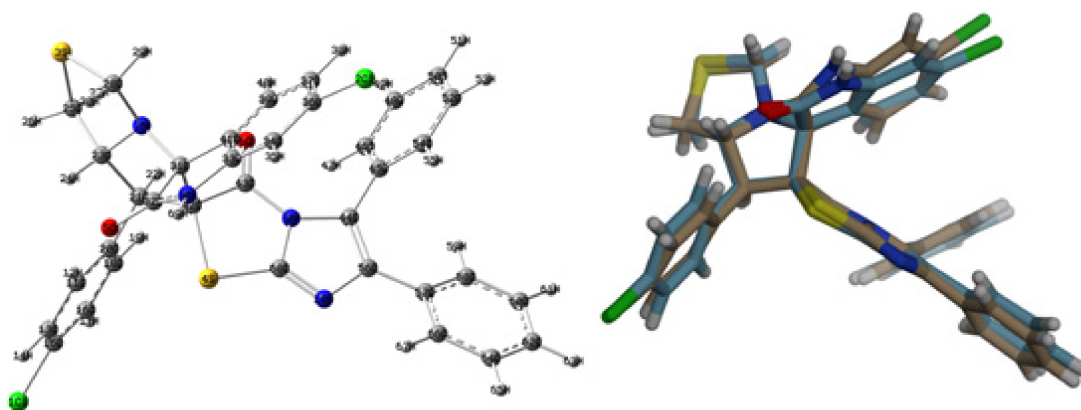


Figure 8. The calculated geometry using a B3LYP method (left) and its overlay with an experimental one (right) for **4**.

The results of the charge calculations indicated the electropositive nature of both S-atoms (Table S2 (Supplementary Data)). It is clear that the S-atom (0.3759 e) located in the five membered ring which contain the carbonyl group, has a higher positive charge than the other S-site (0.1929 e). In addition, the two chlorine atoms have very small natural charges of -0.0040 and 0.0075 e. All nitrogen and oxygen atomic sites are electronegative where the carbonyl oxygen atom of the cyclic amide has the highest negative charge of -0.6032 e. In contrast, the hydrogen atoms have positive charge where the NH proton has the highest positive natural charge of 0.4481 e. The net dipole moment of **4** is calculated to be 3.1664 Debye. In MEP, the intense blue region close to the NH proton reveals its electropositive nature while the intense red regions (most electronegative) are close to the carbonyl oxygen atoms (Figure 10).

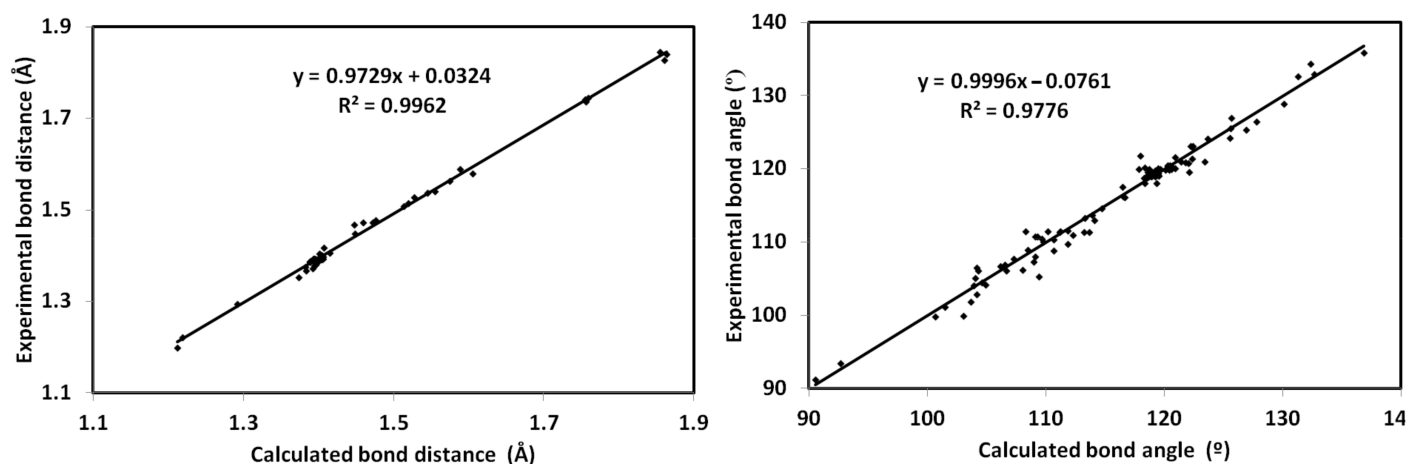


Figure 9. Correlations between the calculated and the experimental geometric parameters.

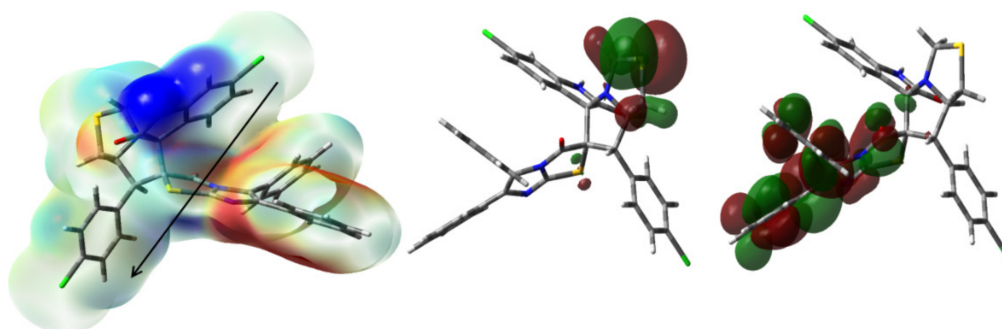


Figure 10. The MEP, HOMO and LUMO of 4. Black arrow indicates the direction of the dipole moment vector.

On the other hand, the HOMO and LUMO presentations are explored in Figure 10. The HOMO level is mainly located over the S-atom of the thiazolidinyl ring while the LUMO one is localized over the π -system of one of the aryl groups which indicate $n\text{-}\pi^*$ excitation for the HOMO \rightarrow LUMO intramolecular charge transfer. Based on the HOMO and LUMO energies, the ionization potential ($I = -E_{\text{HOMO}}$), electron affinity ($A = -E_{\text{LUMO}}$), chemical potential ($\mu = -(I + A)/2$), hardness ($\eta = (I - A)/2$) as well as electrophilicity index ($\omega = \mu^2/2\eta$) were calculated [25–31]. These reactivity parameters are calculated to be 5.6663, 1.8719, -3.7691 , 3.7944 and 1.8720 eV, respectively.

Experimentally, three electronic transitions at 339, 246 and 221 nm in the electronic spectra of the studied molecule were detected as shown in Figure S1 (Supplementary Data). Obviously, the electronic spectra showed very little changes due to solvent effects. The longest wavelength band observed at 335 nm in ethanol was calculated using the TD-DFT calculations at 331.9 nm ($f = 0.031$) which was assigned to the HOMO-2 \rightarrow LUMO (63%)/HOMO-1 \rightarrow LUMO (23%) mixed excitations. Hence, this band could be assigned as mixed $\pi\text{-}\pi^*$ and $n\text{-}\pi^*$ transitions (Figure 11).

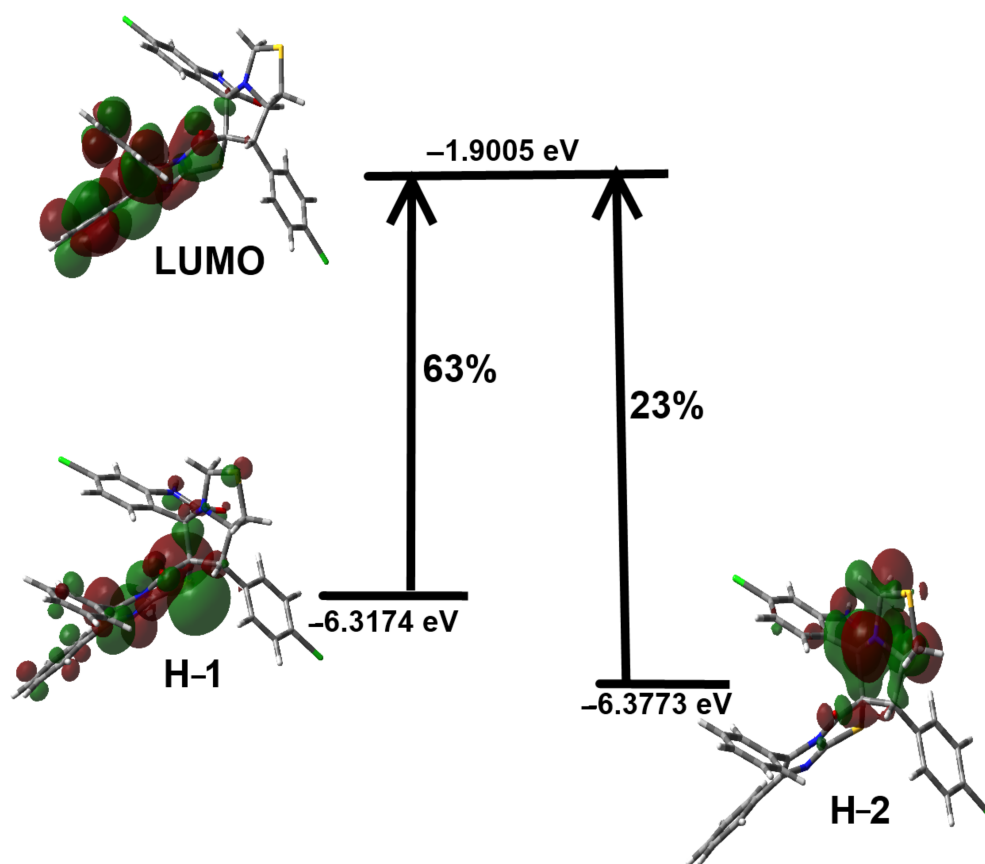


Figure 11. MOs included in the longest wavelength electronic absorption band for the studied system.

On the other hand, NMR calculations were used to compute the ^1H and ^{13}C chemical shifts (Table S3 (Supplementary Data)). In Figure 12, the computed chemical shifts correlated well with the experimental values ($R^2 = 0.96$ – 0.97).

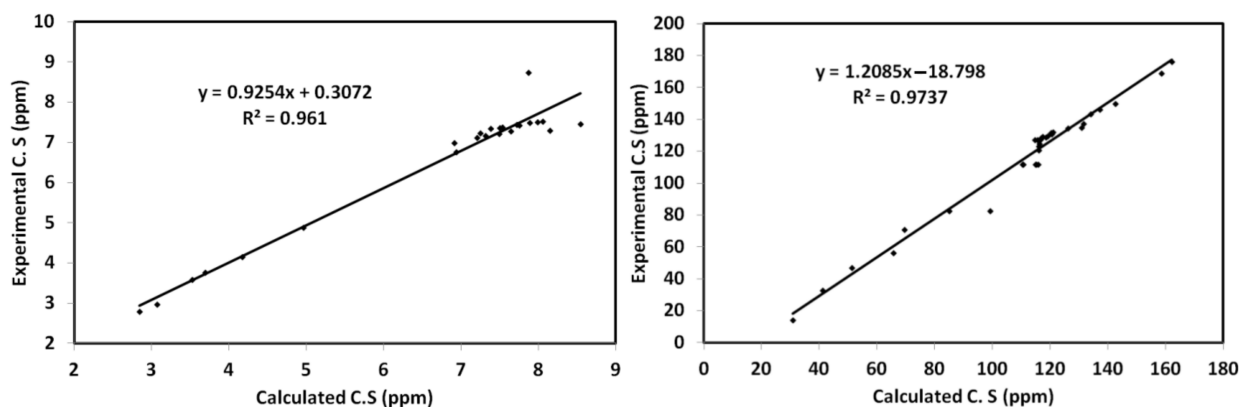


Figure 12. ^1H and ^{13}C NMR correlations between the calculated and experimental data.

4. Conclusions

The new spirooxindole hybrid incorporating the imidazo[2,1-*b*]thiazole derivative was designed, synthesized and elucidated its chemical structure successfully. Based on Hirshfeld calculations, many intermolecular contacts such as $\text{H} \dots \text{H}$, $\text{H} \dots \text{C}$, $\text{Cl} \dots \text{H}$ and $\text{S} \dots \text{H}$, as well as $\text{O} \dots \text{H}$, $\text{N} \dots \text{H}$, $\text{Cl} \dots \text{C}$, $\text{Cl} \dots \text{O}$ and $\text{N} \dots \text{O}$ interactions affect the molecular packing of **4**. The studied compound has polar nature (3.1664 Debye). The NMR chemical shifts correlated well with the experimental results. The UV-Vis electronic

spectral bands observed experimentally were assigned based on TD-DFT calculations. DFT calculations were used to compute the electronic and spectroscopic properties of the studied system.

Supplementary Materials: The following are available online at <https://www.mdpi.com/article/10.3390/cryst12010005/s1>, Figures S1–S4: ¹HNMR, ¹³CNMR, IR and UV-Vis spectrum, Tables S1–S3: computational investigations.

Author Contributions: Conceptualization, A.B.; methodology, M.S.A. and A.A.A.; software, S.M.S. and M.H.; validation, M.S.A., N.H.A.-S., and A.A.A.; formal analysis, M.S.A., N.H.A.-S., M.H., and A.A.A.; investigation, M.S.A.; resources, M.S.A. and A.B.; data curation, A.B., and S.M.S.; writing—original draft preparation, A.B., and S.M.S.; writing—review and editing, A.B., and S.M.S.; visualization, A.B., M.S.A. and N.H.A.-S.; supervision, A.B., and M.S.A.; project administration, A.A.A.; funding acquisition, M.S.A. All authors have read and agreed to the published version of the manuscript.

Funding: This work was funded by the Deanship of Scientific Research at Princess Nourah bint Abdulrahman University, through the Research Groups Program Grant no. (RGP-1443-0040).

Institutional Review Board Statement: Not applicable.

Informed Consent Statement: Not applicable.

Data Availability Statement: Not applicable.

Acknowledgments: This work was funded by the Deanship of Scientific Research at Princess Nourah bint Abdulrahman University, through the Research Groups Program Grant no. (RGP-1443-0040).

Conflicts of Interest: The authors declare no conflict of interest.

References

1. Li, J.J. *Heterocyclic Chemistry in Drug Discovery*; John Wiley & Sons, Inc.: Hoboken, NJ, USA, 2013.
2. Shareef, M.A.; Khan, I.; Babu, B.N.; Kamal, A. A Comprehensive review on the therapeutic versatility of imidazo [2,1-*b*]thiazoles. *Curr. Med. Chem.* **2020**, *27*, 6864–6887. [[CrossRef](#)]
3. Shetty, N.S.; Khazi, I.A.M.; Ahn, C.-J. Synthesis, anthelmintic and anti-inflammatory activities of some novel imidazothiazole sulfides and sulfones. *Bull. Korean Chem. Soc.* **2010**, *31*, 2337–2340. [[CrossRef](#)]
4. Çapan, G.; Ulusoy, N.; Ergenç, N.; Kiraz, M. New 6-phenylimidazo[2,1-*b*]thiazole derivatives: Synthesis and antifungal activity. *Monatsh. Chem.* **1999**, *130*, 1399–1407. [[CrossRef](#)]
5. Cascioferro, S.; Parrino, B.; Petri, G.L.; Cusimano, M.G.; Schillaci, D.; DI Sarno, V.; Musella, S.; Giovannetti, E.; Cirrincione, G.; Diana, P. 2,6-Disubstituted imidazo[2,1-*b*][1,3,4]thiadiazole derivatives as potent staphylococcal biofilm inhibitors. *Eur. J. Med. Chem.* **2019**, *167*, 200–210. [[CrossRef](#)]
6. Sbenati, R.M.; Semreen, M.H.; Semreen, A.M.; Shehata, M.K.; Alsaghir, F.M.; El-Gamal, M.I. Evaluation of imidazo[2,1-*b*]thiazole-based anticancer agents in one decade (2011–2020): Current status and future prospects. *Bioorg. Med. Chem.* **2021**, *29*, 115897. [[CrossRef](#)] [[PubMed](#)]
7. Başoğlu, F.; Ulusoy-Güzeldemirci, N.; Akalın-Çiftçi, G.; Çetinkaya, S.; Ece, A. Novel imidazo [2,1-*b*] thiazole-based anticancer agents as potential focal adhesion kinase inhibitors: Synthesis, in silico, and in vitro evaluation. *Chem. Biol. Drug. Des.* **2021**, *98*, 270–282. [[CrossRef](#)]
8. Potikha, L.M.; Brovarets, V.S. Synthesis of imidazo [2,1-*b*][1,3] thiazoles—potential anticancer agents derived from γ -bromodipnones. *Chem. Heterocycl. Compd.* **2020**, *56*, 1073–1077. [[CrossRef](#)]
9. Li, Y.; Bionda, N.; Fleeman, R.; Wang, H.; Ozawa, A.; Houghten, R.A.; Shaw, L. Identification of 5,6-dihydroimidazo[2,1-*b*]thiazoles as a new class of antimicrobial agents. *Bioorg. Med. Chem.* **2016**, *24*, 5633–5638. [[CrossRef](#)] [[PubMed](#)]
10. Miyazaki, M.; Naito, H.; Sugimoto, Y.; Kawato, H.; Okayama, T.; Shimizu, H.; Miyazaki, M.; Kitagawa, M.; Seki, T.; Fukutake, S.; et al. Lead optimization of novel p53-MDM2 interaction inhibitors possessing dihydroimidazothiazole scaffold. *Bioorg. Med. Chem. Lett.* **2013**, *23*, 728–732. [[CrossRef](#)] [[PubMed](#)]
11. Mona, C.E.; Besserer-Offroy, É.; Cabana, J.; Leduc, R.; Lavigne, P.; Heveker, N.; Marsault, É.; Escher, E. Design, synthesis, and biological evaluation of CXCR4 ligands. *Org. Biomol. Chem.* **2016**, *14*, 10298–10311. [[CrossRef](#)] [[PubMed](#)]
12. Barakat, A.; Islam, M.S.; Ghawas, H.M.; Al-Majid, A.M.; Elsenduny, F.; Badria, F.A.; Elshaier, Y.; Ghabbour, H.A. Design and synthesis of new substituted spirooxindoles as potential inhibitors of the MDM2–p53 interaction. *Bioorg. Chem.* **2019**, *86*, 598–608. [[CrossRef](#)]
13. Altowyan, M.S.; Barakat, A.; Al-Majid, A.M.; Al-Ghulikah, H. Spiroindolone analogues bearing benzofuran moiety as a selective cyclooxygenase COX-1 with TNF- α and IL-6 inhibitors. *Saudi J. Biol. Sci.* **2020**, *27*, 1208–1216. [[CrossRef](#)] [[PubMed](#)]

14. Islam, M.S.; Al-Majid, A.M.; Azam, M.; Verma, V.P.; Barakat, A.; Haukka, M.; Elgazar, A.A.; Mira, A.; Badria, F.A. Construction of spirooxindole analogues engrafted with indole and pyrazole scaffolds as acetylcholinesterase inhibitors. *ACS Omega* **2021**, *6*, 31539–31556. [[CrossRef](#)]
15. Barakat, A.; Alshahrani, S.; Al-Majid, A.M.; Ali, M.; Altowyan, M.S.; Islam, M.S.; Alamary, A.S.; Ashraf, S.; Ul-Haq, Z. Synthesis of a new class of spirooxindole–benzo[*b*]thiophene-based molecules as acetylcholinesterase inhibitors. *Molecules* **2020**, *25*, 4671. [[CrossRef](#)]
16. Zhou, L.-M.; Qu, R.-Y.; Yang, G.-F. An overview of spirooxindole as a promising scaffold for novel drug discovery. *Expert Opin. Drug Discov.* **2020**, *15*, 603–625. [[CrossRef](#)] [[PubMed](#)]
17. Lotfy, G.; Aziz, Y.M.A.; Said, M.M.; El Ashry, E.S.H.; El Tamany, E.S.H.; Abu-Serie, M.M.; Teleb, M.; Dömling, A.; Barakat, A. Molecular hybridization design and synthesis of novel spirooxindole-based MDM2 inhibitors endowed with BCL2 signaling attenuation; a step towards the next generation p53 activators. *Bioorg. Chem.* **2021**, *117*, 105427. [[CrossRef](#)]
18. Aziz, Y.M.A.; Lotfy, G.; Said, M.M.; El Ashry, E.S.H.; El Tamany, E.S.H.; Soliman, S.M.; Abu-Serie, M.M.; Teleb, M.; Yousuf, S.; Dömling, A.; et al. Design, Synthesis, Chemical and biochemical insights into novel hybrid spirooxindole-based p53-MDM2 inhibitors with potential Bcl2 signaling attenuation. *Front. Chem.* **2021**, *9*, 735236. [[CrossRef](#)]
19. Ríos-Gutiérrez, M.; Domingo, L.R. Unravelling the mysteries of the [3+2] cycloaddition reactions. *Eur. J. Org. Chem.* **2019**, *2019*, 267–282. [[CrossRef](#)]
20. Domingo, L.R.; Chamorro, E.; Perez, P. Understanding the high reactivity of the azomethine ylides in [3 + 2] cycloaddition reactions. *Lett. Org. Chem.* **2010**, *7*, 432–439. [[CrossRef](#)]
21. Domingo, L.R.; Kula, K.; Ríos-Gutiérrez, M. Unveiling the reactivity of cyclic azomethine ylides in [3+2] cycloaddition reactions within the molecular electron density theory. *Eur. J. Org. Chem.* **2020**, *2020*, 5938–5948. [[CrossRef](#)]
22. Domingo, L.R.; Ríos-Gutiérrez, M.; Pérez, P. A Molecular electron density theory study of the role of the copper metalation of azomethine ylides in [3+2] cycloaddition reactions. *J. Org. Chem.* **2018**, *83*, 10959–10973. [[CrossRef](#)] [[PubMed](#)]
23. Mustafa, A.; Ali, M.I.; Abou-State, M.A.; Hammam, A.-E.G. Reactions with 4,5-disubstituted 2-mercaptoimidazoles and their derivatives. *J. Prakt. Chem.* **1972**, *314*, 785–792. [[CrossRef](#)]
24. Barakat, A.; Haukka, M.; Soliman, S.M.; Ali, M.; Al-Majid, A.M.; El-Faham, A.; Domingo, L.R. Straightforward regio- and diastereoselective synthesis, molecular structure, intermolecular interactions and mechanistic study of spirooxindole-engrafted rhodanine analogs. *Molecules* **2021**, *26*, 7276. [[CrossRef](#)]
25. Tannor, D.J.; Marten, B.; Murphy, R.; Friesner, R.A.; Sitkoff, D.; Nicholls, A.; Honig, B.; Ringnalda, M.; Goddard, W.A., III. Accurate first principles calculation of molecular charge distributions and solvation energies from ab initio quantum mechanics and continuum dielectric theory. *J. Am. Chem. Soc.* **1994**, *116*, 11875–11882. [[CrossRef](#)]
26. Cheeseman, J.R.; Trucks, G.W.; Keith, T.A.; Frisch, M.J. A comparison of models for calculating nuclear magnetic resonance shielding tensors. *J. Chem. Phys.* **1996**, *104*, 5497–5509. [[CrossRef](#)]
27. Foresman, J.B.; Frisch, M.J. *Exploring Chemistry with Electronic Structure Methods*, 2nd ed.; Gaussian: Pittsburgh, PA, USA, 1996.
28. Chang, R. *Chemistry*, 7th ed.; McGraw-Hill: New York, NY, USA, 2001.
29. Kosar, B.; Albayrak, C. Spectroscopic investigations and quantum chemical computational study of (*E*)-4-methoxy-2-[(*p*-tolylimino)methyl]phenol. *Spectrochim. Acta Part A Mol. Biomol. Spectrosc.* **2011**, *78*, 160–167. [[CrossRef](#)] [[PubMed](#)]
30. Koopmans, T.A. Ordering of wave functions and eigenenergies to the individual electrons of an atom. *Physica* **1933**, *1*, 104–113. [[CrossRef](#)]
31. Parr, R.G.; Yang, W. *Density-Functional Theory of Atoms and Molecules*; Oxford University Press: New York, NY, USA, 1989.